An experimental investigation of a gapless high-lift system using circulation control

K. C. Pfingsten, R. D. Cecora and R. Radespiel
Institute of Fluid Mechanics (ISM), Technische Universität Braunschweig
Bienroder Weg 3, 38106 Braunschweig, Germany
K.C.Pfingsten@gmail.com

Abstract

When air is blown from a slot directly upstream of a flap, the flow over the flap can bear large adverse pressure gradients without separation. This effect is used to design high-lift airfoils with low momentum coefficients of blowing. For experimental assessment of these airfoils a rectangular wing with an aspect ratio of 4.3 was built. The flow around the model in a low speed wind tunnel is analysed using pressure measurements and long distance microscopic particle image velocimetry. To measure the velocity in the vicinity of the slot and next to the surface of the flap the jet is seeded with particles. For Reynolds numbers of about $\mathrm{Re} = 1 \cdot 10^6$ the dimensionless momentum coefficient of the jet and the angle of attack of the airfoil are varied. Numerical simulations of the three-dimensional flow around the circulation control airfoil in the wind tunnel are compared to the experimental data. Good agreement is observed in terms of pressure distributions and velocity profiles.

1 Introduction

In recent years noise pollution from aircraft, especially around airports, has become a huge problem. Hence there is an increasing interest in reducing the noise emitted during take off and landing. The conventional high-lift systems, consisting of slats and slotted flaps, are a major contributor of airframe noise. Therefore a gapless high-lift system without slats has a potential of reducing the overall noise emitted by an aircraft. With active flow control a gapless high-lift device is capable of generating the high lift coefficients needed for climb and landing. For circulation control a small fraction of the cold engine flow is used for blowing. The bleed air is pipelined from the engine to a slot directly upstream of the flap and thus the flow over the flap can bear large adverse pressure gradients without separation. Thus a gapless high-lift device with circulation control can generate the required lift. The low drag coefficients during climb-out, achievable with this powered high-lift system, could also allow for new low-noise trajectories, which would further reduce noise impact on the ground. The absence of slats might allow for laminar flow conditions in cruise flight, thereby reducing the drag in this flight segment. Even taking into account the additional system weight associated with the bleed air distribution for a gapless high-lift system, there is a chance of reducing the total weight of the aircraft and possibly the cost, because slats and fowler systems are no longer needed.

The first experiments using blowing to improve lift were conducted in the thirties of the last century by Bamber [1] as well as Hagedorn and Ruden [2]. Circulation control was first proposed for the flow over a circular cylinder by Davidson [3] and then applied to elliptical airfoils by Kind and Maul [4]. Elliptical airfoils utilising circulation control were also investigated by Stevenson et al [3] and Novak et al [6]. At Technische Universität Braunschweig systematic measurements and theoretical considerations for wings with blown flaps by Thomas [7] and Körner [8] yielded lift increase versus necessary momentum coefficients. The elliptical airfoil with circulation control as well as the internally blown flap were extensively investigated by Englar [9] who could demonstrate good lift-over-drag performance. The first aircraft to demonstrate the high-lift capability of circulation control was a technology demonstrator built by Loth [10]. An experimental investigation using particle image velocimetry to assess the flow around a circulation control airfoil with an elliptical trailing edge as well as the flow around an airfoil with a flap was conducted by Jones et al [11]. These configurations were assessed numerically by Baker and Paterson [12] using two-dimensional RANS simulations. Large-eddy simulations for an elliptical profile with circulation control were performed by Slomski et al [13].

Due to the promising results of preceding numerical simulations by the authors [14] further experimental investigations were conducted to analyse an airfoil with circulation control [15]. As in the preceding experiments the jet was not seeded with tracer particles, the velocity in the jet could not be measured. In the experiments discussed here, the jet flow is seeded to measure the velocity profiles in the vicinity of the slot and on the flap surface using long distance microscopic particle image velocimetry. The special requirements for long distance μPIV are discussed by Kähler et al [16]. Simultaneously, numerical simulations of the wind tunnel experiments are performed. The experimental and numerical results are compared to assess the ability of the used flow solver to simulate the flow around an airfoil with circulation control.

2 Coanda Effect

Profiles with blowing close to the trailing edge use the well known Coanda principle to generate high lift coefficients. If a jet is positioned close to a wall, pressure forces change the path of the fluid elements. Thus the jet is deflected to the surface and becomes a tangential wall jet. The reason for this behaviour is low pressure between the jet and the solid surface. Due to the momentum transport from the jet to the stationary or slowly moving fluid, the flow in the vicinity of the jet is accelerated. Since the wall prevents fluid inflow into the area between the jet and the wall, pressure decreases. The emerging pressure gradient normal to the wall generates a force, which moves the jet flow towards the wall. This effect applies for jets along straight and curved walls and hence tangential blowing can be used to achieve large turning of the flow over airfoils.

Investigations by Englar and Hemmerly [17] showed that the Coanda effect works best when the slot height is about 1% to 5% of the curved surface radius and the slot height is about one to two per mil of the chord length.

The driving parameter for the Coanda effect is the dimensionless momentum coefficient, c_μ, of the jet, which is defined as follows:

$$c_\mu = \frac{v_{jet}\ \dot{m}_{jet}}{\frac{1}{2}\,\rho_\infty\, v_\infty^2\, S}$$

It is important to notice that the increase of the lift coefficient is much higher than the used dimensionless momentum coefficient. So the lift gain is due to flow separation control and super circulation and does not arise because the momentum of the jet is directed downwards.

3 Model Design for Wind Tunnel Experiments

Numerical two-dimensional simulations of the flow around profiles using circulation control were conducted to find favourable geometries with low momentum coefficients. The flow around the circulation control profiles was simulated by solving the Reynolds-averaged Navier-Stokes equations using the DLR hybrid unstructured flow solver TAU, which is based on a finite volume scheme [19, 20]. The code processes meshes with different types of cells and combines the advantages of structured grids to resolve boundary layers with the flexible grid generation of unstructured grids. To accelerate the convergence to steady state, techniques like local time stepping, residual smoothing and multi grid based on agglomeration of the dual-grid volumes are available. All preliminary two-dimensional computations were undertaken assuming the boundary layer to be fully turbulent and with the Spalart-Allmaras [21] turbulence model, which has proven its general capability of computing the flow fields around profiles with circulation control, using simulations of the experimental results achieved by Novak [6] for an elliptical profile with circulation control [22, 23].

As a starting point for two-dimensional investigations of circulation control a modern transonic airfoil was chosen, which can be seen in **Figure 1**. The design of the profile with circulation control has been done in a way to retain the characteristics of the basic profile at cruise conditions. First the x-wise position of the slot is defined, which also determines the length of the flap. Thus the slot is positioned directly upstream of the flap. Upstream of this position the original upper surface is used. Downstream of the slot the upper surface of the flap has to be defined. The results of the numerical two-dimensional simulations for different flap geometries were previously published by the authors [15].

For the wind tunnel tests the upper surface of the flap downstream of the vertical slot is defined as shown in **Figure 2**. The length of the large high-lift flap is set to $c_{flap}/c = 0.3$. This geometry is selected for the following reasons: With the large high-lift flap large lift coefficients can be generated for a given momentum coefficient and even when the blowing fails, reasonable lift coefficients can still be achieved. Low momentum coefficients are here assumed as the most important requirement. When the Coanda radius is hidden in the profile during cruise flight conditions the circulation control profile and the basic airfoil are identical. If the flap is deflected for take off and landing, the Coanda radius appears downstream of the slot. The exact position of the hinge line can be used to obtain continuity in surface slope. This feature is not shown in **Figure 2**.

Note that by doubling the slot height the generated lift is only slightly increased. Therfore here a profile with a small slot height such as $h/c = 0.001$ is preferred compared to a larger slot size, because the lift gain per momentum is larger and (as a rough estimate) the percentage of engine bleed air corresponds to the percentage of overall thrust reduction.

As a reference aircraft for the following consideration, an airplane for 260 passengers, a wing area of $S = 244m^2$ and a maximum take off weight of $m = 134\,t$ is chosen. For take off the reference aircraft needs a high-lift system, which can generate a two-dimensional lift coefficient of about $c_l \approx 2.7$. The large high-lift flap with circulation control can provide the necessary lift for take off with flap deflections of $\eta = 20°$. For landing much higher lift coefficients are needed in combination with large drag coefficients. The reference aircraft requires a necessary two-dimensional lift coefficient of about $c_l \approx 3.7$ for the high-lift system. The preceding two-dimensional numerical simulations for this flow condition showed, that this can be achieved with a flap deflected by $\eta = 40°$, this time for an angle of attack of $\alpha = 4°$ [15]. Therefore the model features a flap deflection angle of $\eta = 40°$ to investigate the most important configuration.

In order to achieve a two-dimensional flow around the circulation controlled airfoil and to keep wall interference as small as possible, the aspect ratio of the model should be large. Therefore the chord has to be as short as possible. On the other hand the Reynolds number should be as large as possible to reduce the influence of low Reynolds number effects. As a reasonable compromise a chord length of $c = 0.3m$ was chosen for the wind tunnel model, which yields an aspect ratio of $\Lambda = 4.3$ and a Reynolds number of $\mathrm{Re} = 1 \cdot 10^6$. A profile with this length also provides sufficient space for the ducting of the pressurised air.

With the geometric parameters defined, an aluminium wind tunnel model was manufactured. The model design is displayed in **Figure 3**. The necessary mass flow of pressurised air used for circulation control is supplied into the model using both lateral sides of the wing. Thereby the total pressure distribution in the duct becomes more homogeneous and symmetrical in spanwise direction. Before wind tunnel testing the uniformity of the static pressure in the plenum in spanwise direction was checked by pressure measurements at five locations in the model. For medium feed pressures corresponding to momentum coefficients around $c_\mu = 0.04$ the mean absolute deviation of the static pressures in the plenum was less than 0.1%.

To analyse the jet distribution in spanwise direction, the dynamic pressure in the jet $0.01m$ downstream of the slot was measured. For that reason a small Pitot tube was traversed in spanwise direction. To always measure the same location inside the jet, the probe was kept in close contact to the wall. The results for a medium feed pressure are plotted in **Figure 4**. Here η is the normalised spanwise coordinate of the probe position. The mean absolute deviation of the dynamic pressure is less than 6.5%. Thus we can assume an almost constant momentum coefficient of the jet in spanwise direction over the whole model, which is an important requirement to obtain two-dimensional flow in the middle of the airfoil. It is important to mention that this data cannot be used to determine the jet velocity, as because of its size the probe measures an averaged pressure over a certain boundary layer height. Measurements of the slot yielded a slot height of $h/c = 0.001$ with a maximum deviation of $\Delta h/c = 0.0001$.

4 Wind Tunnel Experiments

The experimental investigations were conducted in the low speed wind tunnel of the Technische Universität Braunschweig, which is a closed-return atmospheric tunnel with a $1.3m$ x $1.3m$ closed test section. An opening angle of $\gamma = 0.2°$ of the floor and ceiling of the test section compensates for the boundary layer growth. In the measurement section a maximum speed of $55m/s$ can be achieved. A heat exchanger in the settling chamber allows constant flow temperature.

The wind tunnel model with circulation control was investigated at a free stream velocity of $v_\infty = 50m/s$, which results in a Mach number of $\mathrm{Ma}_\infty = 0.15$ and a Reynolds number of $\mathrm{Re} = 1 \cdot 10^6$. To analyse the performance of the airfoil for different momentum coefficients the static pressure of the pressurised air provided by a blower could be varied from ambient pressure to $p_{blower}/p_\infty = 2$. To determine the momentum coefficient of the jet, the mass flow from the slot and the jet velocity are needed. To measure the massflow into the airfoil, a flow measuring device is connected to the piping. When the total pressure and the total temperature of the air in the plenum and the static pressure at the slot are measured, the jet velocity can be computed, using the equations for compressible flow and assuming an isentropic change of state from the plenum to the slot. To account for non isentropic losses an efficiency factor for the expansion was evaluated based on numerical simulations of the flow: $\eta_{expansion} = \Delta h/\Delta h_s = v_{jet}^2/v_{jet,s}^2 = 0.96^2$. Thus the momentum coefficient for all experiments could be computed.

The strong suction peak at the airfoil nose causes large laminar flow separation bubbles with a strong effect on the overall airfoil flow. Therefore a zigzag strip was glued very close to the leading edge. The thickness of this transition strip was chosen as $25\mu m$, by which overtripping could be avoided.

To check for two-dimensional separation behaviour of the airfoil, tufts were attached to the upper surface. The flow separation always started in the centre of the airfoil as there was the highest aerodynamic load and then started to grow towards the side walls.

The pressure distribution around the airfoil was measured for different momentum coefficients. For each analysed momentum coefficient the measurements started at an angle of attack of $\alpha = -5°$. The angle of attack was then gradually increased until the flow separated from the airfoil. The pressure distribution on the model surface was measured by 63 pressure taps, which are positioned in the plane of symmetry of the airfoil. The pressure taps were distributed to offer high resolution at the leading edge and on the Coanda surface to capture the suction peaks with sufficient accuracy. There was also one pressure tap in the trailing edge, which features a thickness of $d/c = 0.004$.

In order to compute the c_p-distribution, the pressure at the ceiling and the floor in the plane of symmetry of the test section at a position of 9.5 chord length behind the airfoil was averaged and used as reference pressure. As the experimental calibration of the freestream velocity by the wind tunnel nozzle factor is affected by the high-lift airfoil in the test section, the velocity in the measurement section is measured at the same position as the reference pressure using two Prandtl tubes.

In **Figure 5** the c_p-distributions for an angle of attack of $\alpha = 0°$ and different momentum coefficients are plotted. Without blowing the flow separates at the very beginning of the flap. For small momentum coefficients like $c_\mu = 0.021$ the flow separates downstream of the Coanda surface. If momentum coefficients greater than $c_\mu = 0.040$ are used the flow stays attached up to the trailing edge. Note that an increase of the momentum coefficient always corresponds to an increase of the circulation around the complete airfoil and not only decreases the pressure on the flap. The stagnation point on the lower surface moves backwards if the blowing is intensified. **Figure 8** shows the c_p-distributions around the wind tunnel model for $c_\mu = 0.045$. If the angle of attack is increased the suction peak at the nose becomes stronger as the stagnation point moves backwards. At the same time the suction peak above the Coanda surface weakens.

Using the measured pressure distribution the force normal to the airfoil chord could be computed. In **Figure 7** the normal force coefficients c_n are shown for seven different momentum coefficients between $c_\mu = 0.021$ and $c_\mu = 0.057$. For comparison the normal force coefficients of the airfoil without blowing are also plotted, here the flow over the flap is fully detached for each angle of attack. When the momentum coefficient of the jet is increased, the normal force is increased as well, whereas the angle of attack, for which the maximum normal force is achieved, decreases. The gain in normal force for increasing the momentum coefficient becomes smaller for higher momentum coefficients. For small momentum coefficients the blowing works as boundary layer control, the momentum of the jet results in a later separation of the flow on the upper surface of the flap. When the flow stays attached up to the trailing edge, the end of boundary layer control is reached; a further increase in jet momentum results in super circulation. For super circulation the normal force is still increased by increasing the momentum coefficient. However, the efficiency of the flow control device $\Delta c_n/\Delta c_\mu$ is reduced. This can be seen in **Figure 8**, where the gain in normal force coefficient is plotted over the corresponding momentum coefficient for an angle of attack of $\alpha = 3°$. For the investigated airfoil super circulation starts for momentum coefficients larger than $c_\mu = 0.040$.

Long distance μPIV was used to measure the velocity field over the flap in the centre of the airfoil. Therefore a Quantel Brilliant double pulsed Nd:YAG laser with an energy of $E = 150mJ$ per pulse was used to illuminate a flow parallel light sheet in the middle of the wind tunnel. Due to the necessary high laser power per volume needed for long distance μPIV, reflections of the laser light become an important issue. To prevent the laser sheet from hitting the airfoil surface at a right angle, the light sheet was tilted by $\gamma \approx 35°$ from the vertical. Thus the reflections from the surface could be reduced. To further reduce the reflections the model surface was polished. The laser sheet had a width of $w = 80mm$ and a thickness of $t = 0.1mm$ to reduce the out of plane component of the measured velocity.

Due to the high spatial resolution in association with μPIV a high concentration of seeding particles is necessary in the area of interest. To achieve this high density of tracer particles in the outer flow, stream-tube seeding was realised by introducing the seeding to the flow in the settling chamber of the wind tunnel by a traversable tube with a streamline fairing. Thus a filament of high density seeding with a diameter of about 50mm is created. The pressure distribution around the airfoil is not changed by the tube. The influence of the traversable tube on the turbulence level was assessed by Kruse [18] and has no significant effect on the current measurements.

To get tracer particles into the jet, a second flow of pressurised air is mixed with the flow from the blower. Before the secondary flow is fed into the main flow, after passing through a seeding generator, it is ducted through a cyclone to remove large tracer particles. Thus the interior of the model could be kept clean and a high quality of the seeding particles in the jet can be assured.

For the computation of the momentum coefficient of the jet this additional mass flow has to be monitored as well. As seeding, oil particles with a diameter of about $1\mu m$ were employed. To reduce window contamination by tracer particles, pressurised air is blown through a slot in the wind tunnel wall upstream of the model.

A LaVision Imager ProX 11M with a resolution of 4008 x 2672 pixels was used to capture the particle images. Fast recording of image pairs is ensured by a minimum frame transfer rate of 250ns. A long-distance microscope (Infinity K2) equipped with two magnifier tubes and the close objective CF1 is employed to obtain the optical magnification necessary to investigate the flow in the vicinity of the slot and on the Coanda surface. For data acquisition and data evaluation, Davis7.2 by LaVision was used.

One set of measurements was done to visualize the velocity field in the vicinity of the slot. Thousand images with a field of view of $17mm$ x $11mm$ were taken for an angle of attack of $\alpha = 0°$ and for momentum coefficients of $c_\mu = 0.026$, $c_\mu = 0.033$, $c_\mu = 0.038$, $c_\mu = 0.044$, $c_\mu = 0.050$ and $c_\mu = 0.055$. For an angle of attack of $\alpha = 3°$ thousand images were taken for momentum coefficients of $c_\mu = 0.026$, $c_\mu = 0.032$, $c_\mu = 0.037$, $c_\mu = 0.043$, $c_\mu = 0.049$ and $c_\mu = 0.055$. Once the particle image acquisition of 1000 image pairs for each measurement was completed, the velocity vector field of the flow around the airfoil had to be determined. After several image preprocessing techniques to improve the particle image quality, the particle displacement evaluation was executed in the next step using a cross correlation scheme. Here a multipass interrogation scheme was applied with decreasing interrogation window size from 128 x 128 pixels down to 64 x 64 pixels, 50% overlap and window shifting and deformation. A spatial resolution of the obtained vector field of $0.14mm$ in both directions was achieved, with the first velocity vector in a distance of $d/c < 0.0005$ to the wall. The resulting set of 1000 vector fields for each measurement was then post-processed. It was necessary to filter out non physical vectors, which would corrupt the results of the ensemble averaging procedure. Only if in at least 250 vector fields a valid vector was found at a certain position an average velocity vector for this position was computed. The computed average flow field in the vicinity of the slot for a momentum coefficient of $c_\mu = 0.037$ and an angle of attack of $\alpha = 3°$ is displayed in **Figure 9**. The boundary layer on the upper surface upstream of the slot as well as the high velocity in the jet can be seen. In **Figure 12** the flow field for a momentum coefficient of $c_\mu = 0.043$ is plotted. It is apparent that the velocity in the boundary layer as well as the velocity in the jet is increased for the higher momentum coefficient.

The second set of images was taken in order to measure the velocity profiles on the Coanda surface downstream of the slot. As the same optical setup was used the vector field yields also a spatial resolution of $0.14mm$ in both directions. The first velocity information is gained in a distance of $d/c < 0.0005$ to the wall. One thousand images with a size of $17mm$ x $11mm$ were taken for the same parameter space as for the first setup. To evaluate the velocity vectors the same algorithm were used as above. The computed average flow field above the Coanda surface for a momentum coefficient of $c_\mu = 0.037$ and an angle of attack of $\alpha = 3°$ is displayed in **Figure 10**. The high velocity in the jet attached to the Coanda surface can be seen. For a momentum coefficient of $c_\mu = 0.043$ the velocity in the jet is further increased, which can be seen in **Figure 13**.

The third set of measurements was done to visualize the velocity field above the end of the flap. Thus it is possible to determine the minimum momentum coefficient necessary to keep the flow attached up to the trailing edge. For this measurement no magnifier tubes were used, thus the window size is increased to $70mm$ x $47mm$. The corresponding spatial resolution is $0.29mm$. Thousand images were taken for an angle of attack of $\alpha = 3°$ and for momentum coefficients of $c_\mu = 0.026$, $c_\mu = 0.032$, $c_\mu = 0.037$, $c_\mu = 0.043$, $c_\mu = 0.049$ and $c_\mu = 0.055$. To evaluate the velocity vectors the same algorithm were used as above, though a multipass interrogation scheme with decreasing interrogation window size from 128 x 128 pixels down to 32 x 32 pixels was applied. If a momentum coefficient of $c_\mu = 0.037$ is used for blowing the flow is not always attached to the flap. As the flow is in the transition from being completely separated and being attached, the average streamlines, which can be seen in **Figure 11**, are still parallel to the surface. However, the low velocity close to the flap surface shows that the flow is not attached to the surface most of the time. The flow field for a momentum coefficient of $c_\mu = 0.043$ is plotted in **Figure 14**. Here the momentum of the jet is high enough to keep the flow attached up to the trailing edge.

5 Numerical Simulation of Wind Tunnel Experiments

The three-dimensional flow around the wing utilising circulation control was simulated by solving the Reynolds-averaged Navier-Stokes equations, using the DLR hybrid unstructured flow solver TAU, as for the two-dimensional simulations used to design the wind tunnel model. To increase the accuracy of the three-dimensional simulations, low speed preconditioning was used. The viscous walls of the test section were also simulated to obtain realistic results for the flow around the wind tunnel model. For efficient flow computations the chimera technique was employed with a local grid defined around the airfoil. The chimera technique allows using an already attained solution as a restart for a following simulation with a different angle of attack. Using the chimera technique to gradually increase the angle of attack, the flow in the vicinity of maximum lift can be simulated correctly.

In **Figure 15** the spatial discretization of the wind tunnel test section can be seen. This hybrid mesh consists of $6 \cdot 10^6$ nodes. The cylindrical mesh around the model is positioned in the cylindrical hole of the background mesh. This local mesh, which is composed of $14 \cdot 10^6$ nodes, is displayed in **Figure 16** and can be rotated around its centreline. This centreline is identical to the axis of rotation of the wind tunnel model. Thus the chimera technique can be used to account for the hysteresis effect of the separation.

The structured area on the surface of the wing has a thickness of 40 cells. On the walls of the wind tunnel 32 prismatic layers were generated. The nondimensional first grid spacing normal to the wall is smaller than 1.5 on most parts of the surface of the wing, except for local values of about 5 at the nose and on the Coanda surface due to the locally very high velocities. In the vicinity of the jet slot and the trailing edge the grid for the numerical simulation is clustered to capture the jet behaviour correctly.

First simulations of the flow field around the wind tunnel model are performed with the standard ***S**palart-**A**llmaras* (SA) turbulence model without any curvature correction. In **Figure 17** the c_p-distribution on the model surface and the surface streamlines are shown for an angle of attack of $\alpha = 0°$ and a momentum coefficient of $c_\mu = 0.045$. Only one half of the symmetric model is shown in **Figure 17**. The backward side in the figure is the location of the wind tunnel side wall. The computed flow field shows that almost two-dimensional flow can be assumed in the middle of the measurement section. To compute the momentum coefficients the jet velocity in the plane of symmetry is mass averaged over the slot height, multiplied by the overall massflow and divided by the wing area and the dynamic pressure of the flow.

In order to compute the c_p-distribution, the pressure at the ceiling and the floor in the plane of symmetry of the test section at a position of 9.5 chord length behind the airfoil was averaged and used as reference pressure, as it was done for the experimental data. In **Figure 18** and **Figure 19** the measured c_p-distributions for a momentum coefficient of $c_\mu = 0.040$ for an angle of attack of $\alpha = -5°$ and $\alpha = 0°$ are compared with the results of the numerical simulations. In **Figure 20** and **Figure 21** the measured c_p-distributions for a higher momentum coefficient of $c_\mu = 0.045$ are compared with the results of the numerical simulations for the same angles of attack as above.

The good agreement of the numerical and the experimental results demonstrates the capability of the SA turbulence model to simulate the flow around a circulation control airfoil with a sharp trailing edge. Unsteady simulations for higher angles of attack have to be conducted to analyse the capability of the SA turbulence model to predict the flow in the proximity of maximum lift.

In **Figure 22 - 24** velocity profiles attained by particle image velocimetry are compared with the simulated velocity profiles at the midspan position of $x/c = 0.690$, $x/c = 0.715$ and $x/c = 0.755$. All velocity profiles shown here are given for an angle of attack of $\alpha = 0°$ and only the velocity component parallel to the surface is shown. At all positions the velocity is increased by increasing the momentum coefficient.

In **Figure 22** the velocity profiles at $x/c = 0.690$ are plotted, which corresponds to a position about $3mm$ upstream of the slot($x/c = 0.7$). For $c_\mu > 0.040$ the flow on the flap is completely attached and the shape of the velocity profiles is well predicted by using the SA turbulence model. Though the curvature of the experimental velocity profiles in the middle of the boundary layer is slightly smaller. In the regime of boundary layer control, when the c_μ is not large enough to keep the flow attached on the complete flap, the discrepancy between experimental and numerical velocity profiles is larger. Here the numerically simulated velocity for $c_\mu = 0.035$ at the edge of the boundary layer differs by 2% from the velocity interpolated from the experimental results for $c_\mu = 0.033$ and $c_\mu = 0.038$. The simulation for $c_\mu = 0.035$ shows a small separation on the edge of the flap, which has only a size of 2% of the chord length. In the experimental results the separation on the flap is already much stronger for this momentum coefficient (see **Figure 5**) and thus the circulation around the airfoil is reduced in the experiment. If a turbulence model is applied, which takes the effect of shear flow curvature into account, as the SARC model (SARC: ***S**palart-**A**llmaras* model for **R**otation and/or **C**urvature effects) [24], the size of the separation for $c_\mu = 0.035$ increases to 5%.

In **Figure 23** the velocity profiles at $x/c = 0.715$ are plotted, which corresponds to a position about

4.5mm downstream of the slot. In these graphs the jet as well as the shear layer above the jet can be seen. Again the numerically simulated velocity for $c_\mu = 0.035$ at the edge of the boundary layer differs by 2% from the velocity interpolated from the experimental results. For the momentum coefficients of $c_\mu = 0.044$, $c_\mu = 0.050$ and $c_\mu = 0.055$ the shape of the shear layer is predicted quite well, but the momentum deficiency caused by the wake of the lip is about 6% larger in the experiment. The maximum jet velocity for $c_\mu = 0.055$ is about 30% higher in the simulations. It can be speculated that the resolution of the μPIV data is not high enough to resolve the jet profile completely that close to the slot, as the jet has a thickness of about 0.3mm at this position.

The velocity profiles on the Coanda surface are shown in **Figure 24** for a position of $x/c = 0.755$, which corresponds to an angle of 40° on the Coanda surface. The shape of the simulated velocity profile fits well to the experimental results. The absolute values get closer to the experimental results if the blowing is increased. For the highest investigated momentum coefficient of $c_\mu = 0.055$ the velocity is about 4% too small in the shear layer and about 7% in the middle of the jet.

6 Conclusions

The experimental investigation of an airfoil with circulation control using an internally blown high-lift flap yields high normal force coefficients at comparably low momentum coefficients. Pressure distributions along the airfoil and μPIV measurements are obtained to establish a data set useful for validating numerical simulation methods. First numerical simulations show a good agreement with the measured data, even if a simple one-equation turbulence model without curvature correction is used. More numerical simulations have to be conducted to see if the same good agreement can be achieved for maximum lift and if the momentum coefficient and the angle of attack for which separation starts can be predicted as well.

Acknowledgments

The present work is performed as a part of the European research project TimpAN (Technologies to IMProve Airframe Noise), which is part of the sixth framework programme. This project is founded by the European Commission and is coordinated by Airbus France. The authors thank the "Norddeutscher Verbund für Hoch- und Höchstleistungsrechnen" (HLRN) for providing the necessary computational resources.

References

[1] Bamber, M.J.: *Wind tunnel tests on airfoil boundary layer control using a backward-opening slot*, NACA Report 385, 1932.

[2] Hagedorn, H. and Ruden, P.: *Windkanaluntersuchungen an einem Junkers-Doppelflügel mit Ausblaseschlitz am Heck des Hauptflügels*, Bericht A 64 der Lilienthal-Gesellschaft für Luftfahrtforschung, 1938.

[3] Davidson, I. M.: *Aerofoil boundary layer control system*, British Patent No.913,754, 1960.

[4] Kind, R. J., Maul, D. J.: *An experimental investigation of a low-speed circulation controlled airfoil*, The Aeronautical Quarterly, Vol. XIX, May 1968, pp.170-182.

[5] Stevenson, T. A., Franke, M. E., Rhynard, W. E. and Snyder J. R.: *Wind-tunnel study of a circulation control elliptical airfoil*, AIAA Journal of Aircraft Vol.14, No. 9, 1977, pp.881-886.

[6] Novak, C. J.,Cornelius, K. C. and Roads R. K.: *Experimental investigations of the circular wall jet on a circulation control airfoil*, AIAA Paper 87-0155, 1987.

[7] Thomas, F.: *Untersuchungen über die Grenzschichtbeeinflussung durch Ausblasen zur Erhöhung des Auftriebes*, Technische Universität Braunschweig, doctoral thesis, 1961.

[8] Körner, H. and Löhr, R.: *Dreikomponentenmessungen am Modell eines leichten STOL-Flugzeuges mit Ausblasen in Flügeltiefenrichtung*, Deutsche Forschungs- und Versuchsanstalt für Luft- und Raumfahrt, DLR-FB 75-74, 1975.

[9] Englar, R. J.: *Overview of circulation control pneumatic aerodynamics: Blown force and moment augmentation and modification as applied primarily to fixed-wing aircraft*, In: Joslin, D., Jones, G. S. (editors): Applications of circulation control technology, Progress in Astronautics and Aeronautics, Vol.214, AIAA, 2006, pp.23-68.

[10] Loth, J. L.: *Advantages of combining BLC suction with circulation control high-lift generation*, In: Joslin, D., Jones, G. S. (editors): Applications of circulation control technology, Progress in Astronautics and Aeronautics, Vol.214, AIAA, 2006, pp.3-21.

[11] Jones, G. S., Yao, C.-S. and Allan, B. G.: *Experimental investigation of a 2D supercritical circulation-cotrol airfoil using particle image velocimetry*, AIAA Paper 2006-3009, 2006.

[12] Baker, W. J. and Paterson, E. G.: *Simulation of steady circulation control for the general aviation circulation control (GACC) wing*, 2004 NASA-ONR Circulation Control Workshop, March 2004.

[13] Slomski, J. F.,Chang, P. A. and Arunajatesan, S.: *Large eddy simulation of a circulation control airfoil*, 2004 NASA-ONR Circulation Workshop, March 2004.

[14] Pfingsten, K. C. and Radespiel, R.: *Numerical Simulation of a wing with a gapless high-lift system using circulation control*, Notes on Numerical Fluid Mechanics and Multidisciplinary Design, Vol. 96, C. Tropea, Springer, Berlin, 2007.

[15] Pfingsten, K. C. and Radespiel, R.: *Experimental and Numerical Investigation of a Circulation Control Airfoil.*, AIAA Paper 2009-533, 47th AIAA Aerospace Sciences Meeting, Orlando, Florida, 2009.

[16] Kähler, C. J., Scholz, U. and Ortmanns, J.: *Wall-shear-stress and near-wall turbulence measurements up to single pixel resolution by means of long-distance micro-PIV*, Exp. Fluids 41,2006, Springer 2006.

[17] Englar, R.J. and Hemmerly, R.A.: *Design of the circulation control wing STOL demonstrator aircraft*, AIAA Journal of Aircraft Vol.18, No. 1, 1981, pp. 51-58.

[18] Kruse, M. and Radespiel, R.: *Measurement of a laminar separation bubble on a swept horizontal tailplane using μPIV*, AIAA Paper 2008-4054, 38th Fluid Dynamics Conference, Seattle, Washington, 2008.

[19] DLR: *Technical Documentation of the DLR TAU-Code*, Institut für Aerodynamik und Strömungsmechanik, Braunschweig, Göttingen, 2006.

[20] Gerhold, T.: *Overview of the hybrid RANS code TAU*, MEGAFLOW-Numerical Flow Simulation for Aircraft Design Vol.89 Springer-Verlag, 2005 (Notes on Numerical Fluid Mechanics and Multidisciplinary Design), pp.81-92.

[21] Spalart, P. R. and Allmaras, S. R.: *A one-equation turbulence model for aerodynamic flows*, AIAA 92-043, 1992.

[22] Pfingsten, K. C., Jensch, C.,Körber, K. W. and R. Radespiel: *Numerical simulation of the flow around circulation control airfoils*, First CEAS European Air and Space Conference, Berlin, 2007.

[23] Swanson, R. C. and Rumsey, C. L.: *Numerical issues for circulation control calculations*, AIAA Paper 2006-3008, 2006.

[24] Shur, M. L. ,Strelets, M. K., Travin, A. K. and Spalart, P. R.: *Turbulence modeling in rotating and curved channels: Assessing the Spalart-Shur correction*, AIAA Journal, Vol.38, No. 5, 2000, pp. 784-792.

Figures

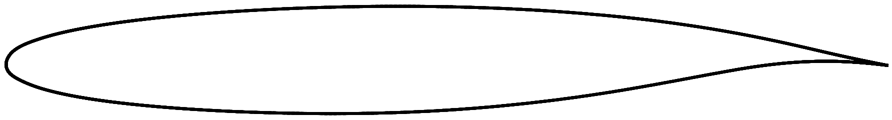

Figure 1: Basic transonic airfoil (not to scale)

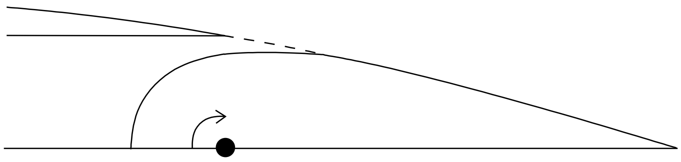

Figure 2: Design of the large high-lift flap

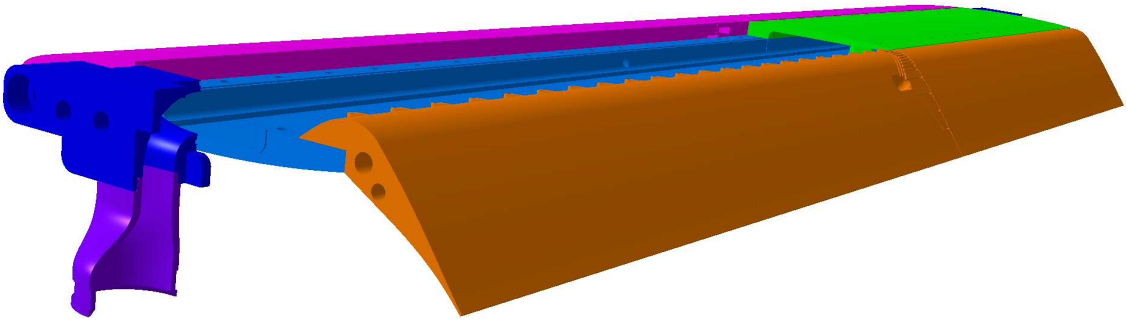

Figure 3: Wind tunnel model with circulation control ducts ($c/c_{flap} = 0.3, h/c = 0.001, \eta = 40°, b/c = 4.3$)

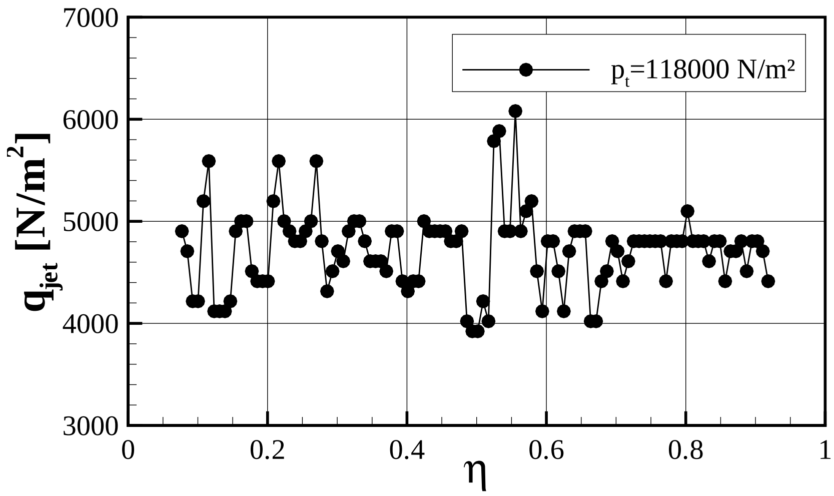

Figure 4: Dynamic pressure distribution in spanwise direction at a position $0.01m$ downstream of the slot

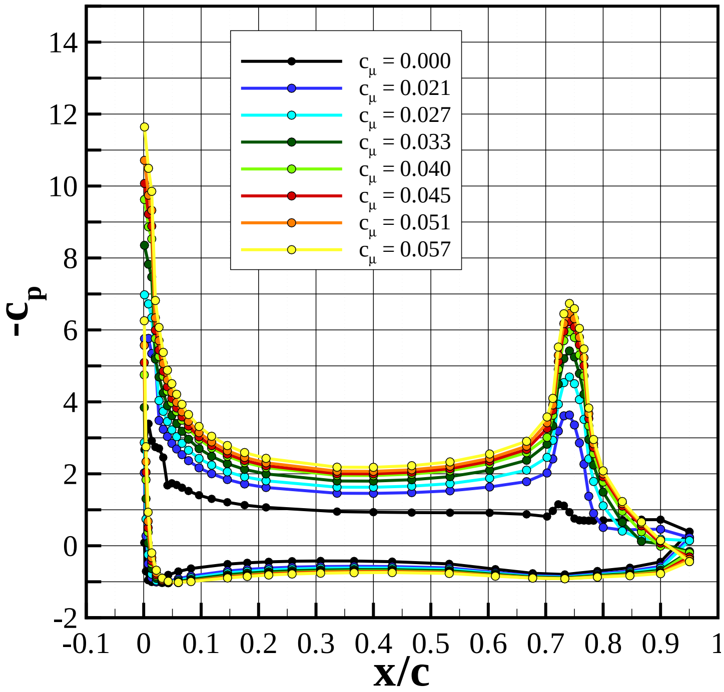

Figure 5: c_p-distribution for $\alpha = 0°$, $\mathrm{Ma}_\infty = 0.15$, $\mathrm{Re} = 1 \cdot 10^6$

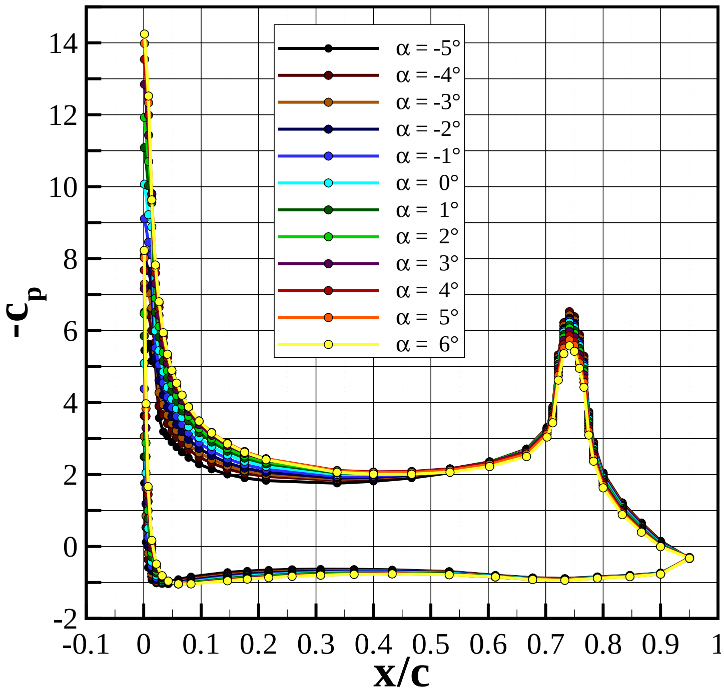

Figure 6: c_p-distribution for $c_\mu = 0.045$, $\mathrm{Ma}_\infty = 0.15$, $\mathrm{Re} = 1 \cdot 10^6$

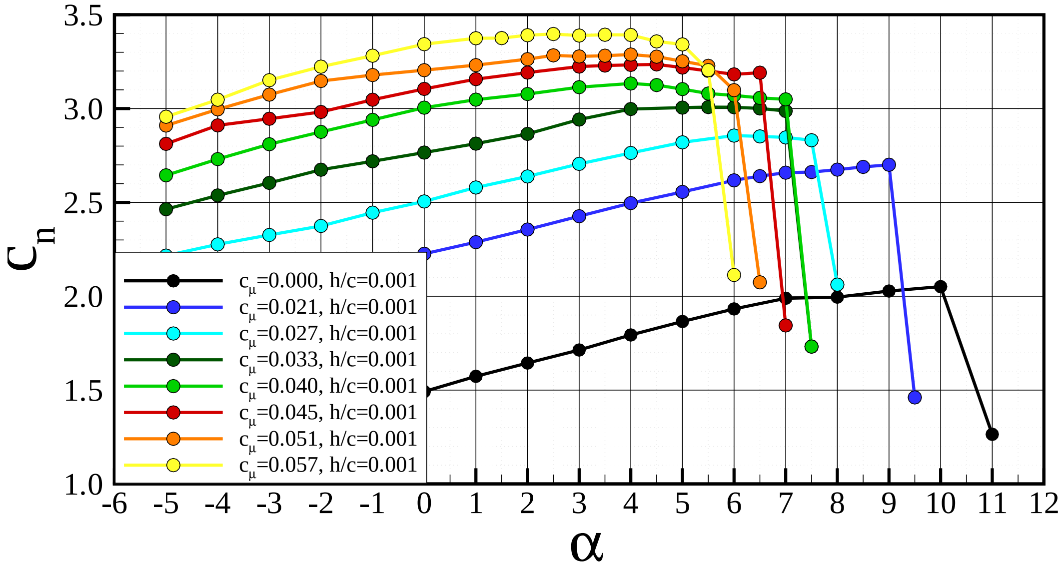

Figure 7: c_n over α for different momentum coefficients ($\mathrm{Ma}_\infty = 0.15$, $\mathrm{Re} = 1 \cdot 10^6$)

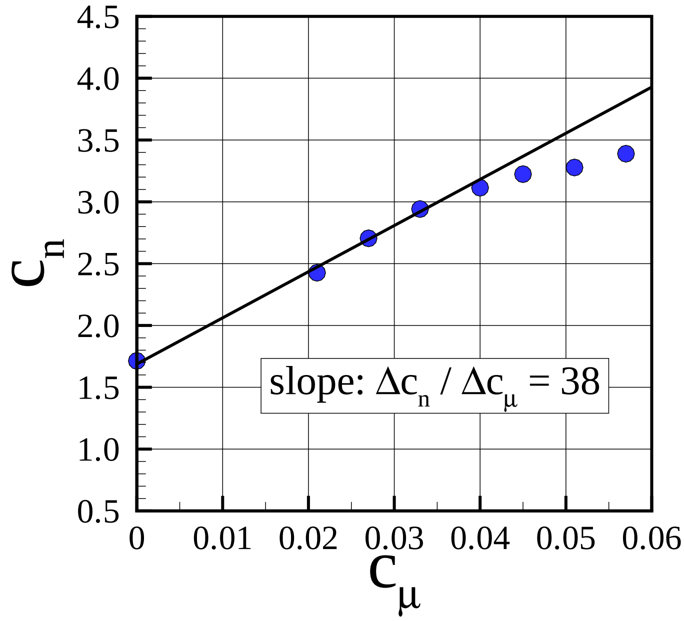

Figure 8: c_n over c_μ for an angle of attack of $\alpha = 3°$ ($\mathrm{Ma}_\infty = 0.15$, $\mathrm{Re} = 1 \cdot 10^6$)

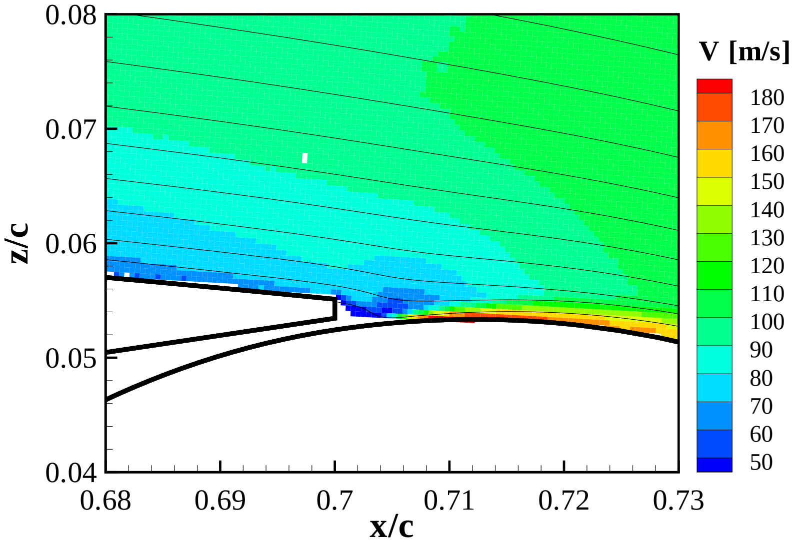

Figure 9: Measured velocity field at the slot for $c_\mu = 0.037$ and $\alpha = 3°$ ($\mathrm{Ma}_\infty = 0.15$, $\mathrm{Re} = 1 \cdot 10^6$)

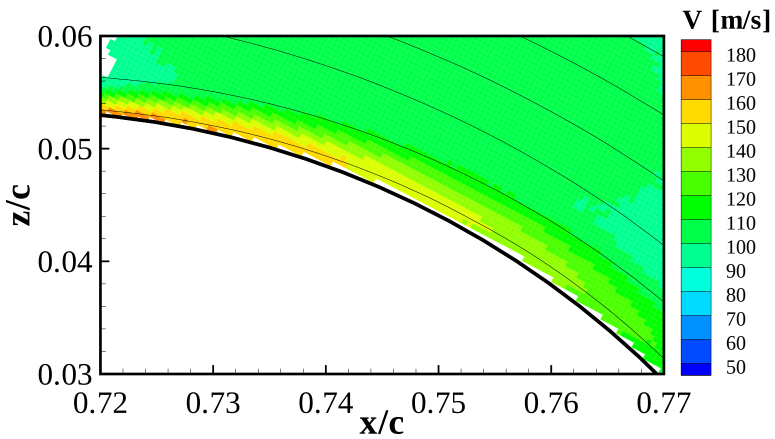

Figure 10: Measured velocity field at the Coanda surface for $c_\mu = 0.037$ and $\alpha = 3°$ ($\mathrm{Ma}_\infty = 0.15$, $\mathrm{Re} = 1 \cdot 10^6$)

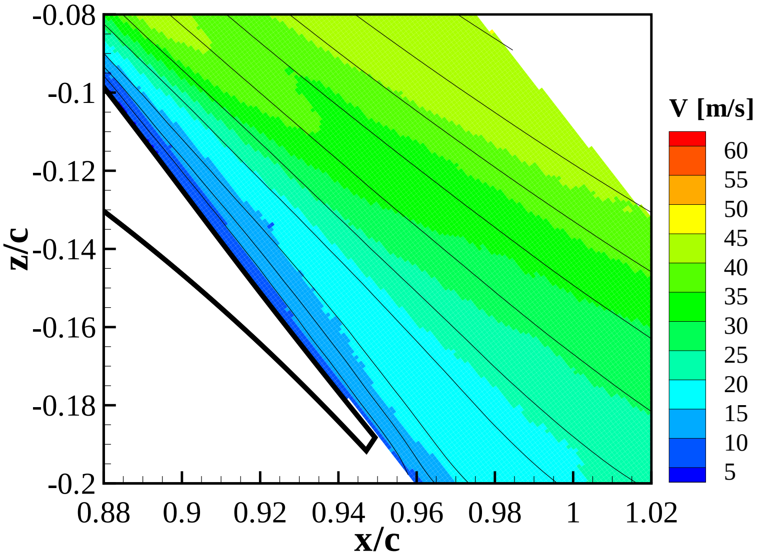

Figure 11: Measured velocity field at the trailing edge for $c_\mu = 0.037$ and $\alpha = 3°$ ($\mathrm{Ma}_\infty = 0.15$, $\mathrm{Re} = 1 \cdot 10^6$)

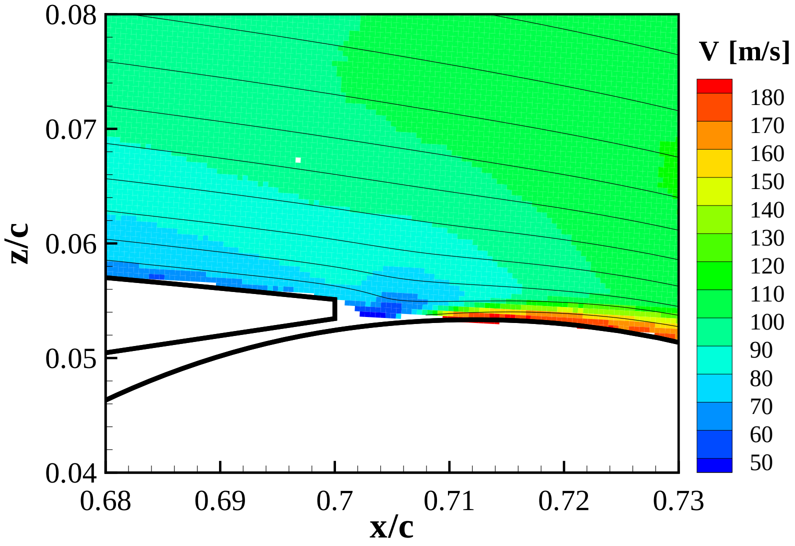

Figure 12: Measured velocity field at the slot for $c_\mu = 0.043$ and $\alpha = 3°$ ($\mathrm{Ma}_\infty = 0.15$, $\mathrm{Re} = 1 \cdot 10^6$)

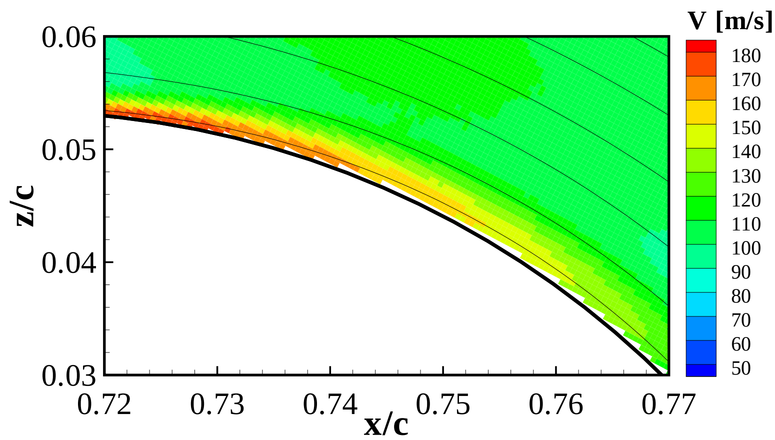

Figure 13: Measured velocity field at the Coanda surface for $c_\mu = 0.043$ and $\alpha = 3°$ ($\mathrm{Ma}_\infty = 0.15$, $\mathrm{Re} = 1 \cdot 10^6$)

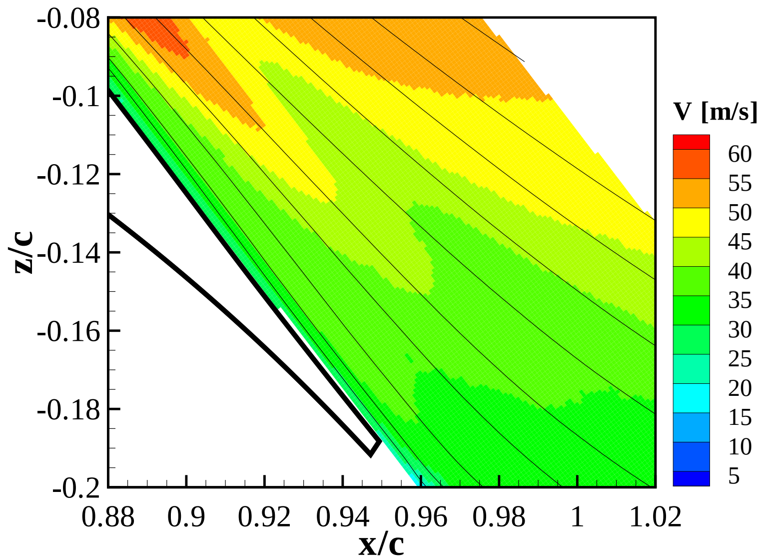

Figure 14: Measured velocity field at the trailing edge for $c_\mu = 0.043$ and $\alpha = 3°$ ($\mathrm{Ma}_\infty = 0.15$, $\mathrm{Re} = 1 \cdot 10^6$)

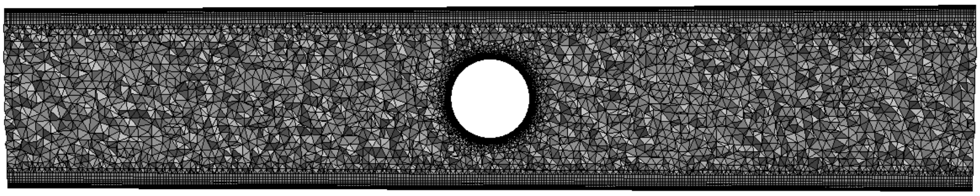

Figure 15: Spatial discretization of the wind tunnel measurement section

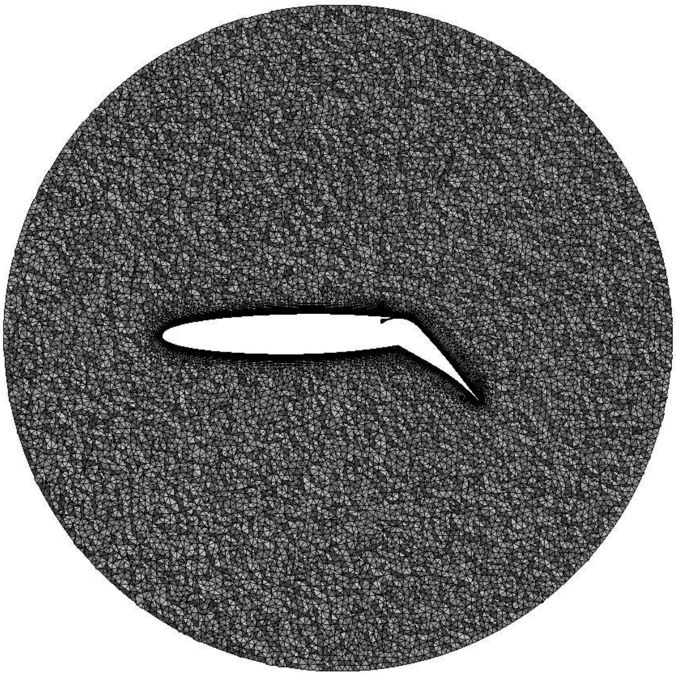

Figure 16: Spatial discretization of the circulation control airfoil

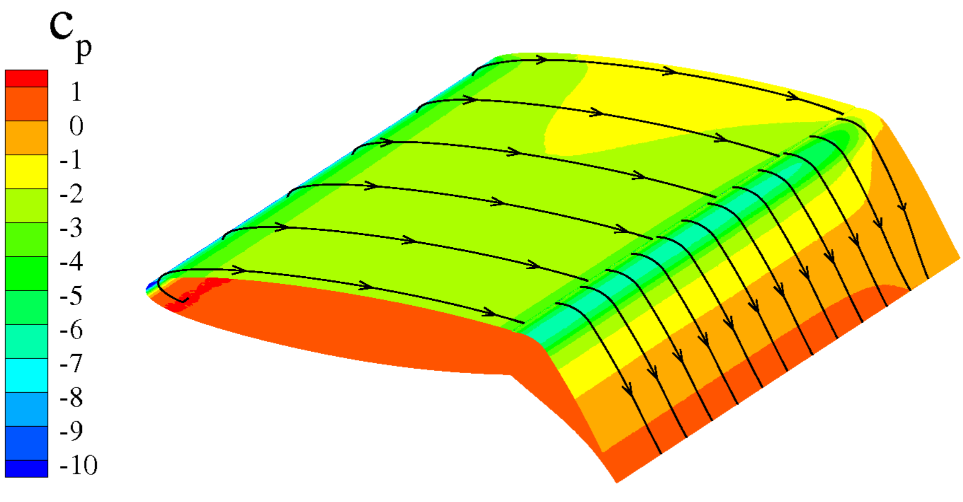

Figure 17: c_p-distribution and surface streamlines on the wing with circulation control:
$\mathrm{Re} = 1 \cdot 10^6$, $\mathrm{Ma} = 0.15$, $c_{flap}/c = 0.3$, $\eta = 40°$, $\alpha = 0°$, $c_\mu = 0.045$, $c_L = 3.04$, $c_D = 0.097$, $c_{M,1/4} = -0.55$

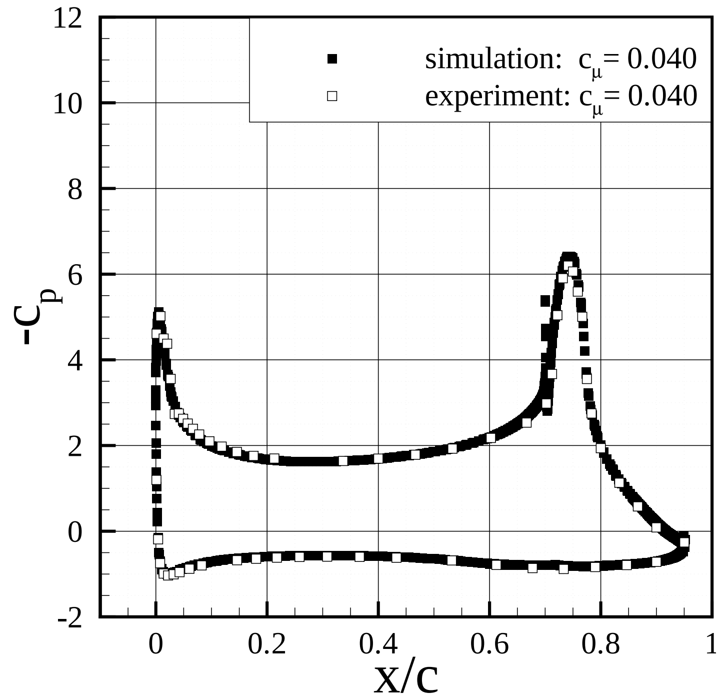

Figure 18: c_p-distribution for $\alpha = -5°$, $\mathrm{Ma}_\infty = 0.15$, $\mathrm{Re} = 1 \cdot 10^6$ (SA turbulence model)

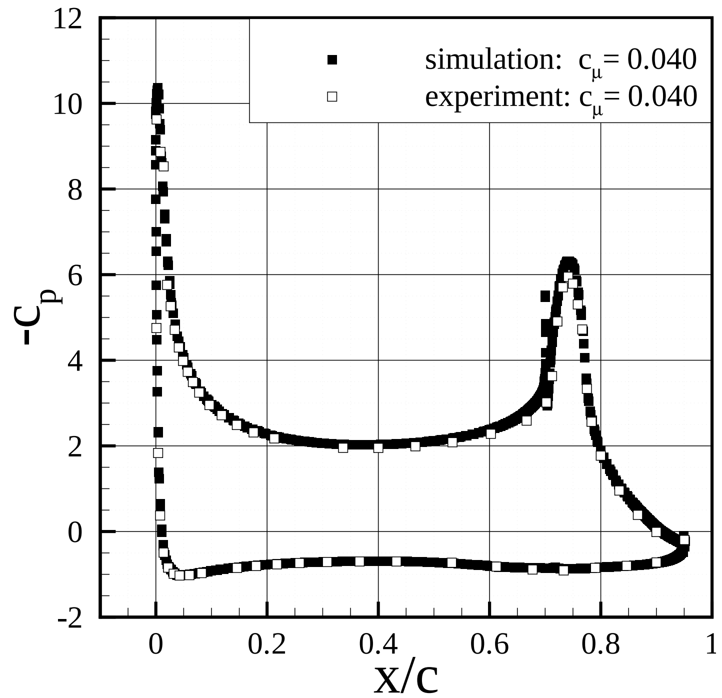

Figure 19: c_p-distribution for $\alpha = 0°$, $\mathrm{Ma}_\infty = 0.15$, $\mathrm{Re} = 1 \cdot 10^6$ (SA turbulence model)

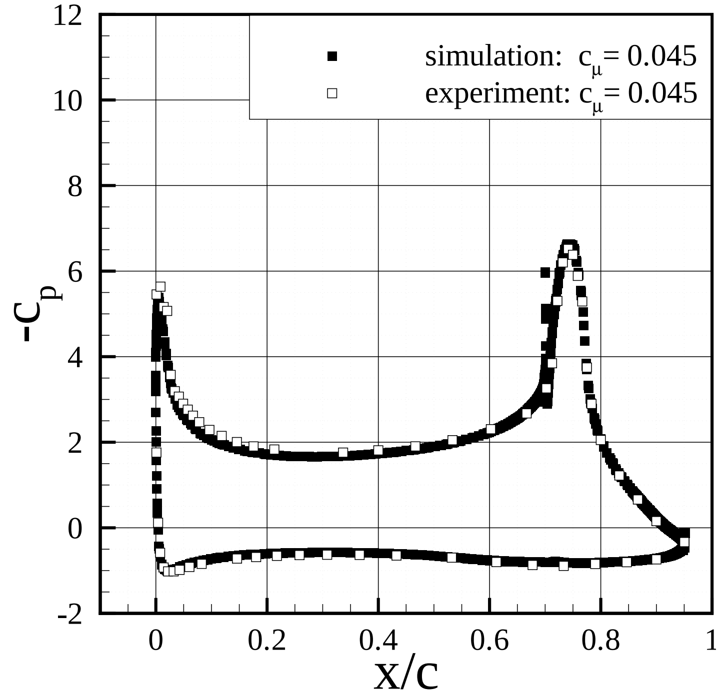

Figure 20: c_p-distribution for $\alpha = -5°$, $\mathrm{Ma}_\infty = 0.15$, $\mathrm{Re} = 1 \cdot 10^6$ (SA turbulence model)

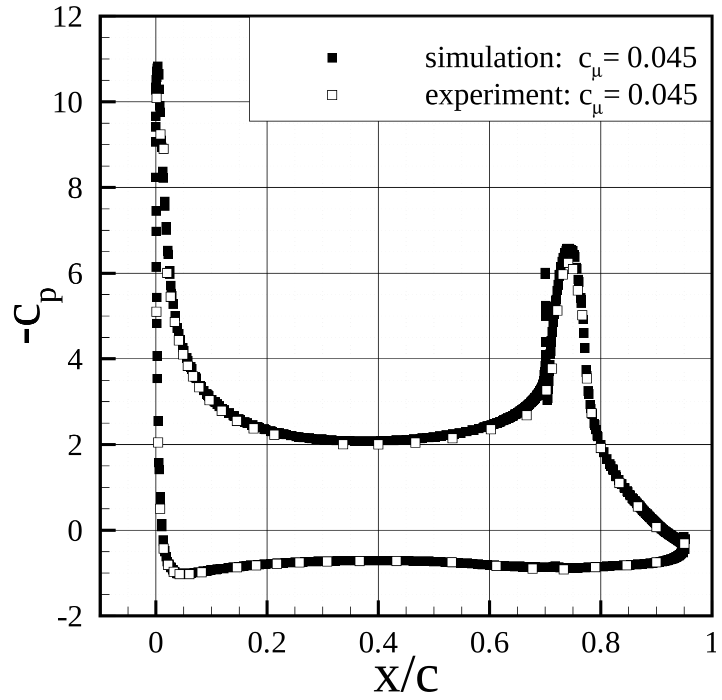

Figure 21: c_p-distribution for $\alpha = 0°$, $\mathrm{Ma}_\infty = 0.15$, $\mathrm{Re} = 1 \cdot 10^6$ (SA turbulence model)

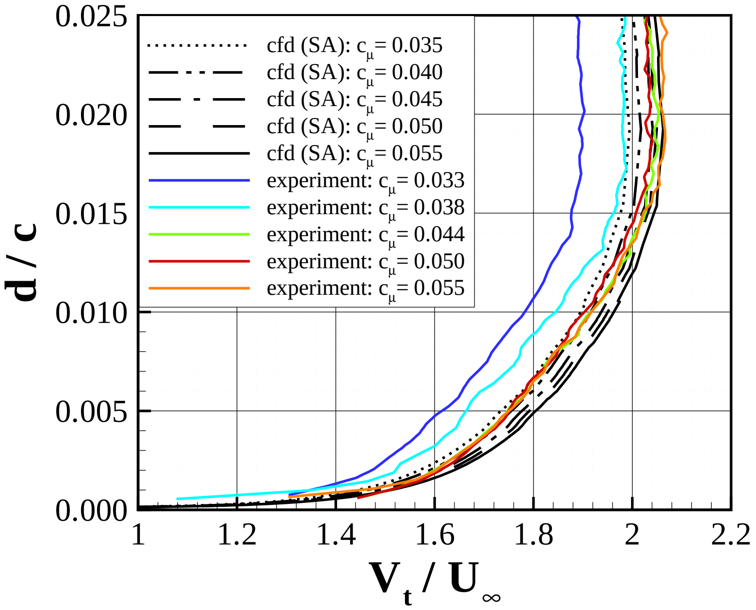

Figure 22: Tangential velocity at $x/c = 0.690$ for $\alpha = 0°$ ($\mathrm{Ma}_\infty = 0.15$, $\mathrm{Re} = 1 \cdot 10^6$)

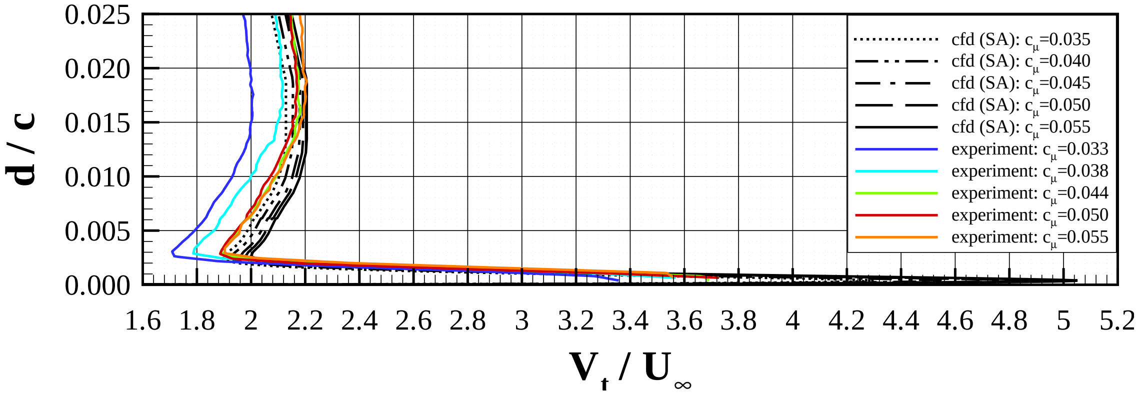

Figure 23: Tangential velocity at $x/c = 0.715$ for $\alpha = 0°$ ($\mathrm{Ma}_\infty = 0.15$, $\mathrm{Re} = 1 \cdot 10^6$)

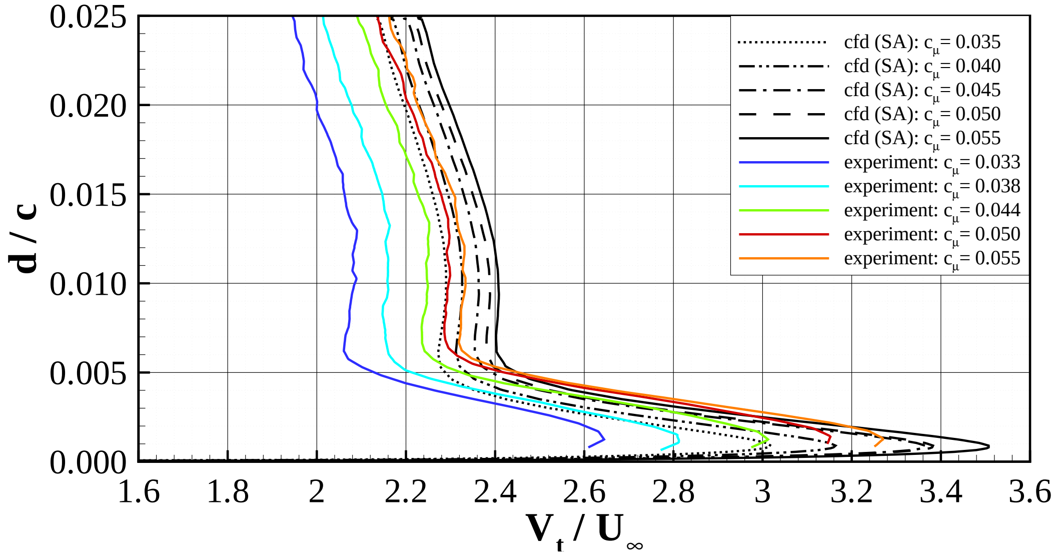

Figure 24: Tangential velocity at $x/c = 0.755$ for $\alpha = 0°$ ($\mathrm{Ma}_\infty = 0.15$, $\mathrm{Re} = 1 \cdot 10^6$)